Analysis of ethanol and butanol direct-injection spark-ignition sprays using two-phase structured laser illumination planar imaging droplet sizing

Koegl, Matthias; Mishra, Yogeshwar Nath; Storch, Michael; Conrad, Chris; Berrocal, Edouard; Will, Stefan; Zigan, Lars

Published in:
International Journal of Spray and Combustion Dynamics

DOI:
10.1177/1756827718772496

2018

Document Version:
Publisher's PDF, also known as Version of record

International journal of spray and combustion dynamics

Original Research Article

International Journal of Spray and Combustion Dynamics
Volume 11: 1–16

DOI: 10.1177/1756827718772496
journals.sagepub.com/home/scd
SAGE

Analysis of ethanol and butanol direct-injection spark-ignition sprays using two-phase structured laser illumination planar imaging droplet sizing

Matthias Koegl[1,2], Yogeshwar Nath Mishra[1,3], Michael Storch[1,2], Chris Conrad[1,2], Edouard Berrocal[2,3], Stefan Will[1,2] and Lars Zigan[1,2]

Abstract

This paper reports on the spray structure of the biofuels, ethanol, and butanol generated by a multihole direct-injection spark-ignition injector, which is studied in a constant volume chamber. The spray shape and structure are analyzed using two-phase structured laser illumination planar imaging where both laser-induced fluorescence and Mie-scattering light are recorded simultaneously for the extraction of instantaneous laser-induced fluorescence/Mie-scattering ratio images. Quantitative planar measurements of the droplet Sauter mean diameter are conducted, using calibration data from phase-Doppler anemometry. The resulting Sauter mean diameters are presented for ethanol and butanol at various fuel temperatures at different times after the start of injection. It is found that an increase in fuel temperature results in a faster atomization and higher evaporation rate, which leads to reduced spray tip penetration and smaller droplet Sauter mean diameter. At equivalent conditions, butanol consistently showed larger spray tip penetration in comparison to ethanol. This behavior is due to the higher surface tension and viscosity of butanol resulting in the formation of larger droplets and larger Sauter mean diameters in the whole spray region. Finally, the butanol injection also shows larger cyclic variations in the spray shape from injection to injection which is explained by the internal nozzle flow that is influenced by larger fuel viscosity as well. The Sauter mean diameter distribution is also compared to phase-Doppler anemometry data showing good agreement and an uncertainty analysis of the structured laser illumination planar imaging-laser-induced fluorescence/Mie-scattering technique for planar droplet sizing in direct-injection spark-ignition sprays is presented.

Keywords

Biofuels, atomization, structured laser illumination planar imaging, laser-induced fluorescence/Mie-scattering ratio, Sauter mean diameter

Date received: 22 December 2017; revised: 29 March 2018; accepted: 30 March 2018

1. Introduction

CO_2 emission limits get constantly stricter over the years. One approach is the intensified usage of biofuels to reduce the overall CO_2 emissions. For this purpose, biofuels such as ethanol and butanol are increasingly blended with conventional gasoline fuel. Yet, under certain circumstances, ethanol- and butanol-blended gasoline can also lead to higher soot formation rates.[1,2] Ethanol blending may lead to a decrease in the evaporation rate due to its large evaporation

[1]Lehrstuhl für Technische Thermodynamik (LTT), Universität Erlangen-Nürnberg, Erlangen, Germany
[2]Erlangen Graduate School in Advanced Optical Technologies (SAOT), Universität Erlangen-Nürnberg, Erlangen, Germany
[3]Division of Combustion Physics, Department of Physics, Lund University, Lund, Sweden

Corresponding author:
Lars Zigan, Friedrich-Alexander-Universität Erlangen-Nürnberg (FAU), Erlangen 91052, Germany.
Email: lars.zigan@fau.de

enthalpy, which could also affect the soot formation and emission. For example, Trost et al.[3] measured a higher evaporative cooling for ethanol compared to the gasoline surrogate fuel iso-octane. Chen and Stone[4] found a continuous increase of particle mass and number with increasing ethanol percentage which also was ascribed to the high evaporation enthalpy. Storch et al.[5] studied ethanol fuel blends in a direct-injection spark-ignition (DISI) spray at simplified cold start conditions (corresponding to late injection timing) within a constant volume chamber. Especially, E20 (single and multicomponent fuels containing 20 vol% of ethanol) showed larger soot volume fractions compared to the pure base fuel (which was observed for iso-octane and a multicomponent gasoline fuel) because of the changed spray processes. In these studies, the soot formation was mainly caused by droplet combustion originating from droplet clouds mostly located at the spray front.[5] It was assumed that mainly large droplets exist in the spray front, which hardly evaporates because of the ethanol content.

Similar effects are expected for fuel blends containing butanol, which is another gasoline biofuel surrogate currently being discussed in the literature. In Knorsch et al.[6] it was found that butanol leads to much larger droplets compared to ethanol and iso-octane, which shows the smallest droplets for ethanol. However, these measurements were made point-wise using a phase-Doppler anemometry (PDA). The sprays were investigated under high ambient temperature conditions (200–400°C, 0.8 MPa) at which the evaporation is predominant and atomization plays a minor role. In the point measurements, there is no spatially resolved information available on the droplet size distribution in the whole spray region. Additionally, low ambient temperature conditions need to be studied as well to identify fuel effects on the atomization behavior. These conditions are predominant under cold start conditions, which significantly contribute to soot formation.

Another relevant research topic is cyclic variations of spray as they determine local mixture composition and, consequently, the subsequent processes ignition and pollutant formation. These spatial and temporal variations are also dependent on fuel properties. For example, Zigan et al.[7] showed that the liquid fuel viscosity plays a major role in the internal nozzle flow and spray propagation and determines cyclic variations in the shape of DISI sprays. These experiments were conducted for alkane fuels (n-hexane, n-decane) under normal ambient conditions (0.1 MPa, 25°C). A low fuel viscosity (large Reynolds number of the nozzle flow) leads to reduced spray cone angle, larger spray penetration, and lower cyclic variation of the spray. Similar effects are expected for biofuels because of the large differences in liquid fuel viscosity.

Thus, further experiments are necessary to clarify the complex, highly turbulent spray processes for ethanol and butanol fuels. New imaging techniques for investigating the spray formation must be capable to provide 2D or even 3D information of the droplet size distribution in the spray and should provide single-shot data of the spray structure to resolve cyclic variations. This cyclic spray motion of engine sprays can have various reasons. The nonstationary, turbulent nozzle flow accompanied with cavitation has a large impact on the spray formation.[8] Furthermore, the spray-induced turbulence in the ambient gas increases cyclic spray variations. This process is also fuel dependent as different atomization and evaporation results in a varied droplet momentum and consequently a varied spray shape and droplet dispersion.

There are a variety of intensity ratio techniques for the 2D mapping of droplet Sauter mean diameter (SMD). For example, the laser-induced fluorescence (LIF)/Mie-scattering (Mie) ratio approach demonstrated by Domann and Hardalupas,[9] the Raman/Mie ratio by Malarski et al.,[10] and Exciplex-LIF/Mie ratio technique by Zeng et al.[11] However, while imaging dense sprays, the conventional intensity ratio approaches suffer from multiple light scattering effects, which may introduce large systematic uncertainties. The temporally averaged structured laser illumination planar imaging (SLIPI) in combination with LIF/Mie ratio technique has been used to mitigate most of these effects.[12] It was shown that the multiple scattering suppression is required even for the sprays having singly scattered photons in majority. Therefore, with SLIPI-LIF/Mie ratio approach, averaged SMD mapping of droplets is extracted in hollow cone water sprays.[12] Recently, the novel two-phase SLIPI (2p-SLIPI) for instantaneous LIF/Mie ratio imaging has been demonstrated in turbulent DISI engine sprays.[13] The 2p-SLIPI technique is based on the use of two spatially modulated light sheets, having the same spatial frequency but opposite spatial phase. It enables qualitative instantaneous LIF/Mie droplet sizing for realistic, highly fluctuating DISI engine sprays, but no quantitative 2D droplet sizing was performed so far. After calibration of the SLIPI-LIF/Mie ratio images representing a qualitative map can be converted to absolute SMD maps. These instantaneous 2D SMD distributions obtained using SLIPI-based ratio provide a deeper and a better insight into the turbulent spray formation of DISI engine sprays in comparison to conventionally acquired 2D droplet distributions.

This paper reports the investigation of spray formation and droplet sizing of ethanol and butanol fuels using 2p-SLIPI in combination with LIF/Mie ratio for droplet sizing. The atomization and evaporation behavior of multijet DISI sprays are investigated in

an injection chamber. The influence of the biofuels ethanol and butanol and fuel temperature on the spray structure and cyclic variation of spray is analyzed. For this purpose, first, the effects of different fuels and temperature on the LIF/Mie ratio are studied. Then, the calibration of the SLIPI-LIF/Mie ratio is conducted using a PDA setup. Finally, the SLIPI-LIF/Mie ratio is used for determination of the 2D SMD distribution in ethanol and butanol sprays. The calibrated SMD data are also compared with droplet SMD acquired by PDA and an uncertainty analysis of the SLIPI-LIF/Mie technique for DISI spray characterization is presented.

2. SLIPI-LIF/Mie droplet sizing

SLIPI is an imaging technique for suppressing multiple light scattering effects, which are common in optically dense sprays.[14,15] In contrast to conventional laser sheet imaging, SLIPI images give a more faithful representation of spray structures. Compared to a homogeneous light sheet illumination in conventional imaging, the incident light sheet with SLIPI follows a sinusoidal pattern. Inspired from the structured illumination microscopy,[16] the technique requires a minimum of three phase-modulated images (subimages) for the reconstruction of a SLIPI image of the sample. The three-phase SLIPI (3p-SLIPI) has been applied for temporally averaged as well as for the instantaneous measurements of sprays.[15] Spray quantities such as droplet SMD,[12] droplet temperature,[17] and extinction coefficient[18,19] were measured with the averaged 3p-SLIPI by recording liquid LIF and/or Mie optical signals. Recently, 2p-SLIPI setups,[13,20] which are based on acquiring two instead of three subimages, have been reported. Thereby, factors limiting the instantaneous 3p-SLIPI application, i.e. complex optical design, use of advanced laser system, and intensified multiframe cameras can be circumvented. The 2p-SLIPI has been demonstrated for capturing transient events in continuously injected hollow cone sprays[20] and for cyclic variations between different injections in engine sprays[13] in terms of the relative SMD. However, still, a calibration of the SLIPI-LIF/Mie ratio is necessary for providing absolute SMD in DISI sprays and effects of different fuels and temperature on the LIF/Mie ratio need to be resolved which is part of this study.

A brief description of the 2p-SLIPI technique is given in the subsequent paragraph for clarity. To generate a 2p-SLIPI image, two incident illuminations encoded with same spatial frequency ν, but mismatched phases are recorded. If two acquired subimages are corresponding to the intensities I_0 and I_π, then the absolute value of their difference is deduced, resulting in an intermediate image. Due to the subtraction of intensities, the regions sharing the same values appear as *residuals*, i.e. with nearly zero intensity. These residual lines are removed by adequately postprocessing the intermediate images in the Fourier domain. The resulting 2p-SLIPI image is therefore extracted as

$$I_{2p-SLIPI} = F_{2\nu}\left(\sqrt{(I_0 - I_\pi)^2}\right) \quad (1)$$

where $F_{2\nu}$ denotes the applied Fourier filtering where the frequency 2ν is suppressed, while $I_{2p\text{-}SLIPI}$ is the light intensity corresponding to the resulting 2p-SLIPI image. A detailed description of the postprocessing of the intermediate image in the Fourier domain can be found in Storch et al.[13] and Mishra et al.[21]

In Figure 1, the 2p-SLIPI postprocessing at 2552 µs after electrical start of injection (aESOI) for an ethanol spray is illustrated. The first two pictures are modulated subimages of phases $\Phi = 0$ and π together with zoomed views. The third and fourth images represent the absolute values of the subtracted images $(I_0 - I_\pi)$, without and with the Fourier filter, respectively. In their zoomed areas, the former one appears with residuals whereas the latter one is free from residuals, which is the final 2p-SLIPI image.

The 2p-SLIPI-LIF/Mie ratio was used in transient DISI sprays[13] for determination of the relative SMD of the fuel spray droplets by the division of simultaneous acquired LIF and Mie images. The theory is based on the assumption that the liquid LIF and Mie signals from dye-doped spherical droplets are

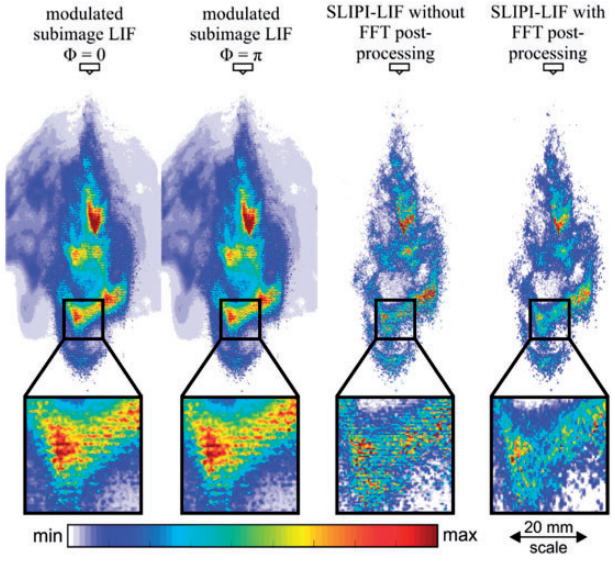

Figure 1. Illustration of postprocessing to extract a 2 p-SLIPI LIF image for ethanol at 2550 µs aESOI and a fuel temperature of 298 K. FFT: fast fourier transform; LIF: laser-induced fluorescence; SLIPI: structured laser illumination planar imaging.

proportional to the droplet volume (d^3) and to their surface area (d^2), respectively.[22] If the majority of photons reaching the camera sensor are singly scattered, the SMD of droplets for each camera pixel can be calculated by

$$SMD = \frac{\sum_0^\infty D_i^3}{\sum_0^\infty D_i^2} = \frac{S_{LIF}}{S_{Mie}} \cdot \frac{K_{LIF}}{K_{Mie}} \quad (2)$$

Here, S_{LIF} and S_{Mie} are the liquid LIF and Mie signals, respectively, while K_{LIF} and K_{Mie} are coefficients corresponding to the experimental parameters such as detector response, laser power, signal collection angle, and dye concentration. Several experimental and theoretical studies have found the d^3 and d^2 dependence of droplet diameter (d) on the LIF and Mie signals, respectively, is not practically valid for larger droplets and higher dye concentrations.[9,23–27]

Regarding the LIF/Mie ratio[12,13,28] it is found that the multiple scattering effects generated from LIF and Mie detections are not the same, thus it is necessary to suppress the multiple light scattering intensity prior to intensity ratio of the two signals, e.g. by application of the SLIPI technique. To deduce the droplet absolute SMD, the calibration of SLIPI-LIF/Mie ratio is necessary, e.g. by SMD data acquired by a PDA system, see, for example Mishra et al.[12]

In the present study, the solid organic luminescent dye Eosin-Y (Kingscote chemicals, USA) is added to the liquid fuel for the LIF experiments. In general, the concentration of the added dye affects the LIF signal in many ways. An increase in dye concentration changes the molecular absorption and the exponent for the fluorescence may vary from three to two.[29] Furthermore, the droplet size distribution has an influence on the proportionality exponent of the LIF signal intensity averaged on an ensemble of droplets. Thus, a low dye concentration should be used. In previous work, the authors found that a tracer concentration of 0.5 vol% Eosin-Y in the liquid fuel fulfills this requirement. It should be noted that in case of evaporation of the fuel the dye concentration in the droplet could change. However, for the studied conditions, the evaporation rate is low and no strong variation of the dye concentration in the droplet is expected (see also discussion below).

The temperature dependency on the fluorescence must also be known which was investigated in a preliminary study for liquid solution from 296 to 324.1 K. The liquid solution of Eosin-Y and ethanol in a cuvette was excited at 532 nm using a continuous wave laser while the spectrum was recorded using an AvaSpec-USB2 spectrometer (version 7.6.1). The integration time was 200 ms and 10 spectra were averaged for determination of the emission curves. The broadband

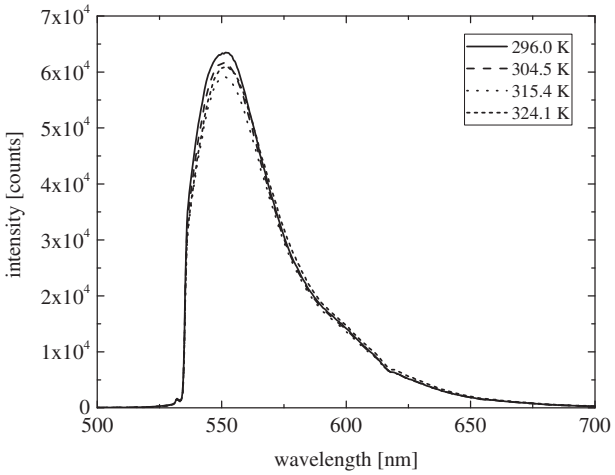

Figure 2. LIF spectra of Eosin-Y (0.5 vol%, dissolved in ethanol) excited at 532 nm at various temperatures.

LIF emission of the liquid solution occurs between 540 and 680 nm for all temperatures (see Figure 2).

The temperature dependence of the LIF signal is negligible since the emission spectrum is not shifted or broadened. Only the peak intensity shows small variations (less than 7% in absolute intensity) in the studied temperature range. This overall signal is relevant as the complete emission spectrum is detected in the LIF measurements. Further discussion regarding dye concentration and temperature changes in evaporating sprays can be found in subsection 4.4.

3. Description of the experiment

The 2p-SLIPI optical setup for simultaneous imaging of the liquid LIF and the Mie signals is shown in Figure 3. A set of two subimages for each detection is acquired by using two scientific CMOS cameras (type Imager, LaVision GmbH). Each acquired subimage is represented by 2560×2160 pixels. For simultaneous recording and for obtaining the same image field of view on both cameras, an in-house camera stage with a single objective is constructed. On the back of the objective, a cube beam splitter (70% reflection, 30% transmission) is placed which distributes the incoming signals onto the two cameras. For the illumination of the spray two pulsed 532 nm Nd:YAG lasers (laser 1, Quanta Ray; and laser 2, Quantel Brilliant) with matched laser fluence and top hat beam profile are used. The pulse duration is in the order of 6 ns, while the pulse repetition rate is 10 Hz. The lines pattern on the light sheets is imprinted through a transmission Ronchi grating with a spatial frequency of four line pairs/mm.

The two overlapping incident laser sheets have a height of 90 mm and a thickness of approximately 500 μm. The time delay between the two laser pulses

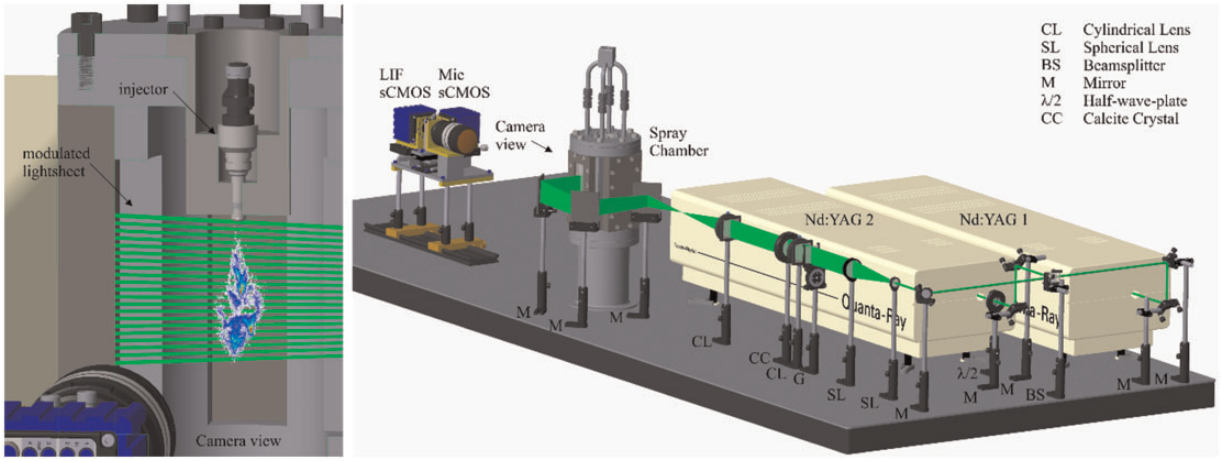

Figure 3. Illustration of the 2p-SLIPI-LIF/Mie experimental setup. CMOS: scientific complementary metal-oxide-semiconductor; LIF: laser-induced fluorescence.

is set to 750 ns, while the two cameras are running in double exposure mode. The short time difference allows the recording of the pair of subimages, required to generate the 2p-SLIPI image while freezing the spray motion. Between the two subimages, the modulated light sheet has to be shifted spatially by 180°. The spatial phase shift is achieved by exploiting the double refraction property of a calcite crystal for two crossed polarized beams. The phase shifting using calcite is described in detail in Storch et al.[13] The different polarization of the beams does not introduce uncertainties to the LIF and Mie signal (for the investigated spray, the droplet size distribution range is 5–20 µm and the Mie simulations show the same light intensity both for *p* and *s* polarization for this diameter range). The fluorescent tracer, Eosin-Y is added at 0.5 vol% of the liquid fuels, ethanol and butanol. The LIF emission is detected by using a 532 nm (17 nm FWHM) notch filter just in front of the sCMOS chip to exclude the excitation light. The Mie signal is detected by using a 532 nm (1 nm FWHM) laser line filter.

The spray chamber is operated with dry air at 0.2 MPa and 293 K, which represents an early injection (during the suction stroke) at a high load engine operating point. The injector and fuel are heated by a fluid-based heating circulator. The temperature of the nozzle tip is measured with a highly sensitive micro sheathed thermocouple (0.25 mm diameter, type K). It is assumed that the fuel adopts the injector temperature due to the long residence time of the fuel in the injector (the injection duration is relatively short—it is kept constant at 1800 µs—for an injection repetition rate of 1 Hz). For the shown experiments, fuel temperatures of 293 and 343 K are adjusted and the injection pressure is set to 8 MPa. This fuel temperature variation should lead to small changes in the spray shape as well as droplet size distributions and with this study, the sensitivity of the SLIPI technique is tested to resolve these variations. The investigated temperature range is also relevant for cold and warm start conditions of the IC engine. A five-hole DISI injector (BOSCH) is utilized, where one jet is centrally separated from the others allowing unrestricted optical access. In this study, ethanol and n-butanol are investigated. The main physical parameters of the fuels are listed in Table 1 at temperatures 293 and 343 K.

Table 1. Physical and chemical properties of ethanol and n-butanol.[30–34]

Fuel	Ethanol	n-butanol
H/C ratio/O/C ratio	3.0/0.5	2.5/0.25
Normal boiling point (K)	351.5	390.9
Density (g/cm^3) @ 298 K, 0.2 MPa	0.801	0.794
Density (g/cm^3) @ 343 K, 0.2 MPa	0.750	0.753
Surface tension @ 293 K (N/m)	0.0223	0.0247
Surface tension @ 343 K (N/m)	0.0180	0.0209
Heat of vaporization @ 293 K (kJ/kg)	929.6	632.9
Heat of vaporization @ 343 K (kJ/kg)	847.1	587.4
Kin. viscosity @ 298 K, 0.2 MPa (m^2/s)	1.30E-06	3.30E-06
Kin. viscosity @ 343 K, 0.2 MPa (m^2/s)	6.51E-07	1.28E-06
Refractive index at 293 K (–)	1.36	1.4

Ethanol and butanol are characterized by very similar density, while the kinematic viscosity and surface tension of butanol are significantly larger for butanol.

Based on the physical and chemical properties of ethanol and n-butanol, the Reynolds number *Re* and the Weber number *We* can be calculated according to

$$Re = \frac{d \cdot u}{\nu_L} \tag{3}$$

Table 2. Weber numbers and Reynolds numbers of ethanol and n-butanol at 293 and 343 K, respectively, at 0.2 MPa.

Fuel	Ethanol	n-butanol
We @ 293 K	86,900	77,800
We @ 343 K	101,000	87,100
Re @ 293 K	15,500	6110
Re @ 343 K	31,000	15,800

Table 3. SMD according to the model of Hiroyasu and Arai[35] for various temperatures.

Fuel (K)	Ethanol (μm)	Butanol (μm)
293	10.2	12.4
343	6.53	9.51

SMD: Sauter mean diameter.

$$We = \frac{d \cdot \rho_L \cdot u^2}{\sigma_L} \tag{4}$$

where d is the nozzle diameter, u is the jet velocity, ν_L is the liquid kinematic viscosity, ρ_L is the liquid fuel density, and σ_L is the surface tension of the liquid fuel. With a nozzle diameter of 168 μm and an estimated jet velocity of $u = 120$ m/s (determined in Storch et al.[2] at similar conditions), the We and corresponding Re can be deduced (see Table 2). An increase of the temperature leads to an increase in We of about 11–16%. More significant are the changes in Re that are more than doubled for a temperature increase of 50 K. For ethanol, the Re is about two times larger compared to n-butanol.

According to a model proposed by Hiroyasu and Arai,[35] the resulting SMD (of a diesel spray) mainly depends on We, Re, and dynamic viscosity μ (see equation (5), Table 3). While larger We leads to smaller SMD, larger fuel viscosity leads to larger SMD

$$SMD = 4.12 Re^{0.12} We_L^{-0.75} \left(\frac{\mu_L}{\mu_G}\right)^{0.54} \left(\frac{\rho_L}{\rho_G}\right)^{0.18} \cdot d \tag{5}$$

In this equation, μ_L is the liquid dynamic viscosity, μ_G is the dynamic viscosity of the ambient gas, and ρ_G is the density of the ambient gas.

It can be concluded that ethanol will produce smaller SMD due to smaller Re and larger We. Furthermore, the expected SMD is reduced for both fuels at increasing temperature due to lower Re and higher We. At the same time, ethanol shows a lower boiling point. Thus, ethanol should evaporate faster; however, the high evaporation enthalpy of ethanol could lead to a stronger cooling of the ambient gas, which would again reduce the evaporation rate of droplets entering these colder regions.

For all experiments, identical image readout and postprocessing routine is conducted. At each operating point, 200 instantaneous images were taken and averaged afterward. For calibration and comparison of the SLIPI LIF/Mie ratio, the SMD of the fuel spray was measured within a PDA equipped chamber. The PDA system is a FiberPDA (Dantec Dynamics A/S) combined with an Innova 305 C Laser (Coherent Inc.). The laser beams were overlapped in an intersection volume by transmitter optics using a 310 mm collimation lens. The resulting probe volume length was 468 μm and the diameter was 45 μm. The volume contained 15 fringes with a fringe spacing of about 2.67 μm. This setup leads to a measurement range of droplet sizes up to 50 μm. The probe volume was positioned within the spray using a 3D traversing unit. The signal bursts were detected by an optical receiver equipped with a lens of 310 mm focal length and a receiving aperture mask for small particles. The aperture slit limits the effective measurement volume's length to 100 μm. The Brewster angle of 70° was chosen for signal detection. This detection scheme is less sensitive to changes in refractive index of the different fuels (see also Table 1) at different fuel temperatures.

For every measurement location, a maximum of 10,000 validated droplets was collected corresponding up to 120 injections. The SMD is determined at different locations within the fuel spray. The PDA measurement pattern is shown in Figure 4.

Regions very close to the nozzle tip are discarded, as the LIF/Mie ratio (and PDA) is not applicable in this region because of the presence of irregular ligaments (that disappear after few 100 μm) and nonspherical drops (which exist due to secondary breakup and droplet coalescence further downstream). Thus, for the evaluation of the LIF/Mie data only the measurement points at a distance beyond 40 mm from the nozzle are considered.

4. Results and discussion

This section is structured in four subsections. First, for the qualitative evaluation, single-shot images of ethanol and butanol are discussed in terms of the SLIPI-LIF/Mie ratio. From that, averaged images and the coefficient of variation (COV, or relative standard deviation) are calculated to visualize the cyclic variability of these sprays. Afterward, the temperature effect on relative SMD and cyclic spray variations is discussed. In the next section, the SLIPI-LIF/Mie ratio is calibrated

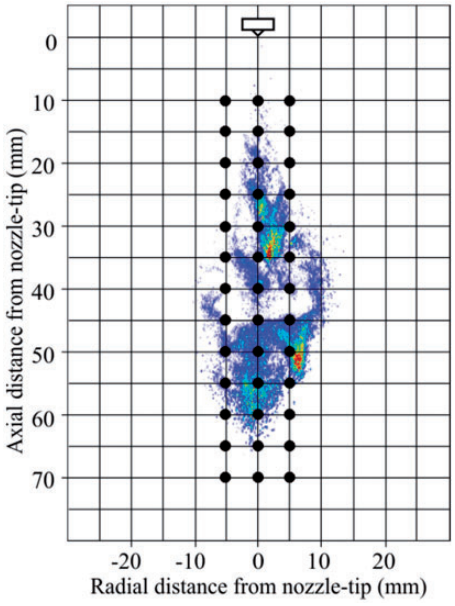

Figure 4. PDA measurement positions within a single image of an ethanol spray at 2552 μs aESOI at 8 MPa injection pressure and 343 K fuel temperature. COV: coefficient of variation; LIF: laser-induced fluorescence; SLIPI: structured laser illumination planar imaging.

using absolute SMD data from PDA measurements. The fuel-dependent calibration curves are presented and 2D maps of droplet SMD distributions are discussed for ethanol and butanol in the whole spray region. In the final section, an uncertainty analysis is presented.

4.1. LIF/Mie data for ethanol and butanol

Figure 5 shows the three instantaneous images of the LIF and Mie and their corresponding LIF/Mie ratio both for the ethanol (E100, left) and butanol sprays (B100, right). The turbulent spray structure can be visualized only with instantaneous images while fluctuations in the spray shape and the vortex structures are not visible in the mean images. A good indication of cyclic variation is provided by the COV (right columns). The acquisition time is fixed to 2552 μs aESOI for all the cases. The modulated light sheets enter the spray from the left side and illuminate the central jet of the multijet spray. When comparing the LIF and the Mie images obtained using SLIPI it is noticed that a strong signal occurs at the spray front in both cases. The signal of the LIF/Mie ratio also shows the largest intensities at the spray front and on the radial edges of the spray, which indicates larger droplets. The drag forces at the spray front support collision of the fuel droplets accompanied with droplet coalescence. This leads to larger droplets at the spray front, which are still present at the studied late points in time. This effect is typical for DISI sprays.[36,37]

Large cavities produced by large turbulent eddies are visible behind the spray front. These are characterized by a low LIF/Mie ratio in their center corresponding to small droplets. The evaporation of fuel may also lead to low LIF/Mie signals of the droplets in these spray regions. When comparing ethanol and butanol sprays, it is evident that the butanol sprays have larger penetration depth and a slightly smaller spray angle. The larger penetration is caused by the formation of larger droplets mainly due to the higher viscosity and surface tension of butanol. This leads to higher droplet momentum and reduced droplet deformation and breakup, thus lower surface-specific drag forces. This fuel-dependent spray structure is discussed in terms of SMD distribution after calibration in subsection 4.3.

4.2. Spray shape at different fuel temperatures

In Figures 6 and 7, comparisons of the averaged LIF/Mie ratios and the COVs are shown for ethanol and butanol at two different fuel temperatures (293 and 343 K) at different recording times aESOI. With increasing fuel temperature, the axial spray penetration is reduced while the radial spray width increases slightly. In general, the butanol sprays showed a larger axial penetration compared to ethanol. An increase of the fuel temperature leads to smaller SMD (as mentioned above) because of stronger atomization and increased evaporation rate, which is visible in the reduced LIF/Mie ratio, especially at the spray front. This results in reduced droplet momentum and thus to a reduced spray tip penetration.

At the same time, a rather wider spray plume results for a fuel temperature of 343 K. The same trends are observable for butanol (see Figure 7).

Similar results were reported by Aleiferis et al.[38] who studied E85 and gasoline spray propagation also at different fuel temperatures. They also found a reduced penetration with increasing fuel temperature, especially at low gas pressures. In general, it can be noted that these fuel temperature effects lead to distinct changes in the spray structure and relative droplet sizes, which can be resolved by the 2 p-SLIPI-LIF/Mie ratio technique.

The penetration depth of ethanol is almost constant over time at 343 K, whereas for butanol it increases constantly with time. The larger droplet size of butanol leads to larger axial droplet momentum and thus to a higher spray tip penetration in comparison to ethanol.

The COV maps (in the right columns in Figure 7) show no significant fuel temperature effects. In general, the highest fluctuations appear at the spray front and

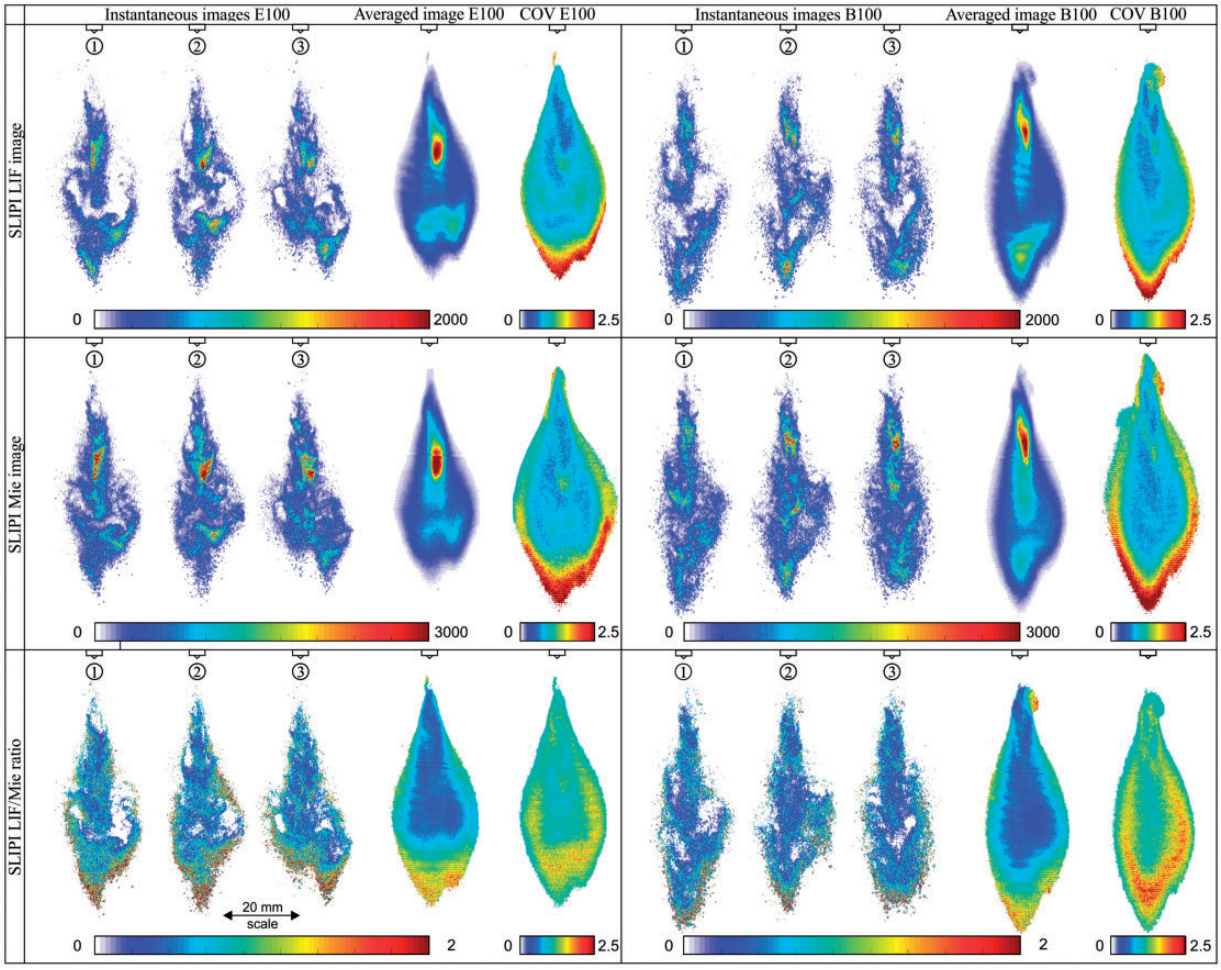

Figure 5. Instantaneous and averaged images of ethanol (E100) and butanol (B100) as well as the COV, 2552 µs aESOI, 343 K fuel temperature. COV: coefficient of variation; LIF: laser-induced fluorescence; SLIPI: structured laser illumination planar imaging.

lateral spray boundary, which is obvious from the single-shot measurements displayed in Figure 5. Butanol sprays showed larger maximal values of the cyclic variations in comparison to ethanol. This behavior could be caused by the large fuel viscosity of butanol (and thus smaller Reynolds numbers of the internal nozzle flow). Similar behavior was also observed by Zigan et al.[7] for different n-alkane fuels studied at comparable conditions for a DISI injector. Compared to a homogeneous light sheet illumination in conventional imaging, the incident light sheet with SLIPI follows a sinusoidal pattern. For higher Reynolds numbers the flow and spray were more reproducible because of the higher turbulence inside the injection hole.[7] However, for the present work, no information about the nozzle flow is available and this aspect must be considered in future studies. Furthermore, the spray-induced turbulence could be larger for butanol as well (due to larger droplets and droplet momentum) which intensifies cyclic variations in the spray.

4.3. Comparison between ethanol and butanol spray structure in terms of SMD

In order to convert SLIPI-LIF/Mie ratio into absolute SMD maps a calibration process is required. The calibration is usually done either by using PDA data from point-wise measurements or by using single droplet LIF/Mie ratio data of known droplet size from a droplet generator. For this study, the calibration of the SLIPI-LIF/Mie ratio was performed with PDA measurements. Furthermore, PDA data were used for validation of the SLIPI results in the whole spray region as well. The PDA data are received continuously in time, and for calculation of the SMD, the droplet sizes are averaged over a ±50 µs period. Averaged data from all three points in time (2302, 2552, and 2802 µs) and 200 injections for each fuel are used for calculating the corresponding SLIPI-LIF/Mie ratio. Corresponding to the PDA measurement position, in each LIF/Mie ratio image 9×9 pixels (370×370 µm) are spatially averaged. Here, measurement positions 40–70 mm away

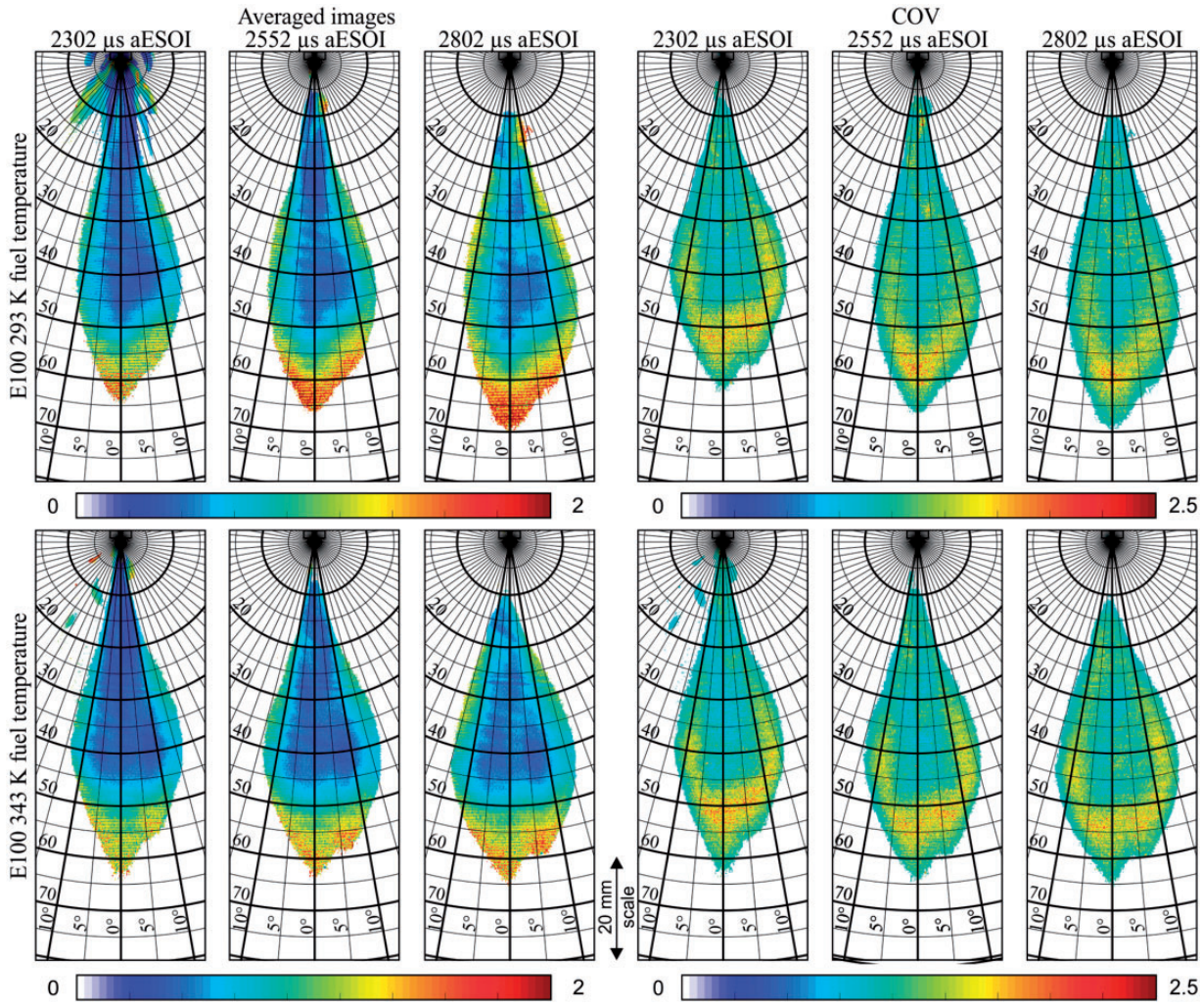

Figure 6. Comparison of averaged SLIPI-LIF/Mie ratio (left) and its corresponding COV (right) for ethanol at fuel temperatures 293 and 343 K and at 2302, 2552, and 2882 µs aESOI. COV: coefficient of variation; aESOI: after electrical start of injection.

from the nozzle tip were considered as indicated in Figure 4.

The large cyclic variations in spray shape and LIF/Mie ratio occur at the spray front (see Figures 6 and 7) and thus these data were not used in the SLIPI-LIF/Mie ratio calibration. The plots of LIF/Mie ratio plotted against the SMD (acquired by PDA) are shown in Figure 8.

The slope of calibration curves shows a fuel-dependent behavior. This is mainly due to the different spectral fluorescence emission behavior of eosin in different solvents, i.e. ethanol and butanol in this case. In general, eosin in ethanol shows a higher fluorescence intensity over the whole emission range than eosin in butanol as it is also reported in Chakraborty and Panda.[39] It was also reported previously that different fuels (especially ethanol) strongly affect the fluorescence intensity of other LIF tracers (e.g. triethylamine) in the liquid phase, which does not occur for alkane-based fuels. This effect is explained by the interaction of the tracer and ethanol molecules leading to the lower fluorescence intensity of ethanol compared to the signal intensity of iso-octane.[40] From this, it follows that a comparison of the LIF/Mie ratio between different fuels is only possible using a fuel-specific calibration curve as given in Figure 8.

Finally, these calibration curves are used for discussion of the SMD distribution in the whole spray region in the subsequent paragraphs.

A comparison of the planar droplet size distribution of ethanol and butanol is displayed in Figure 9 for three different points in time. Furthermore, the PDA data are plotted in the respective measurement points in the spray region.

In general, the SMD distribution of the PDA data and the calibrated LIF/Mie ratio show a good agreement for both fuels. The SLIPI-derived SMD and PDA data fit very well in the center of the spray, in which

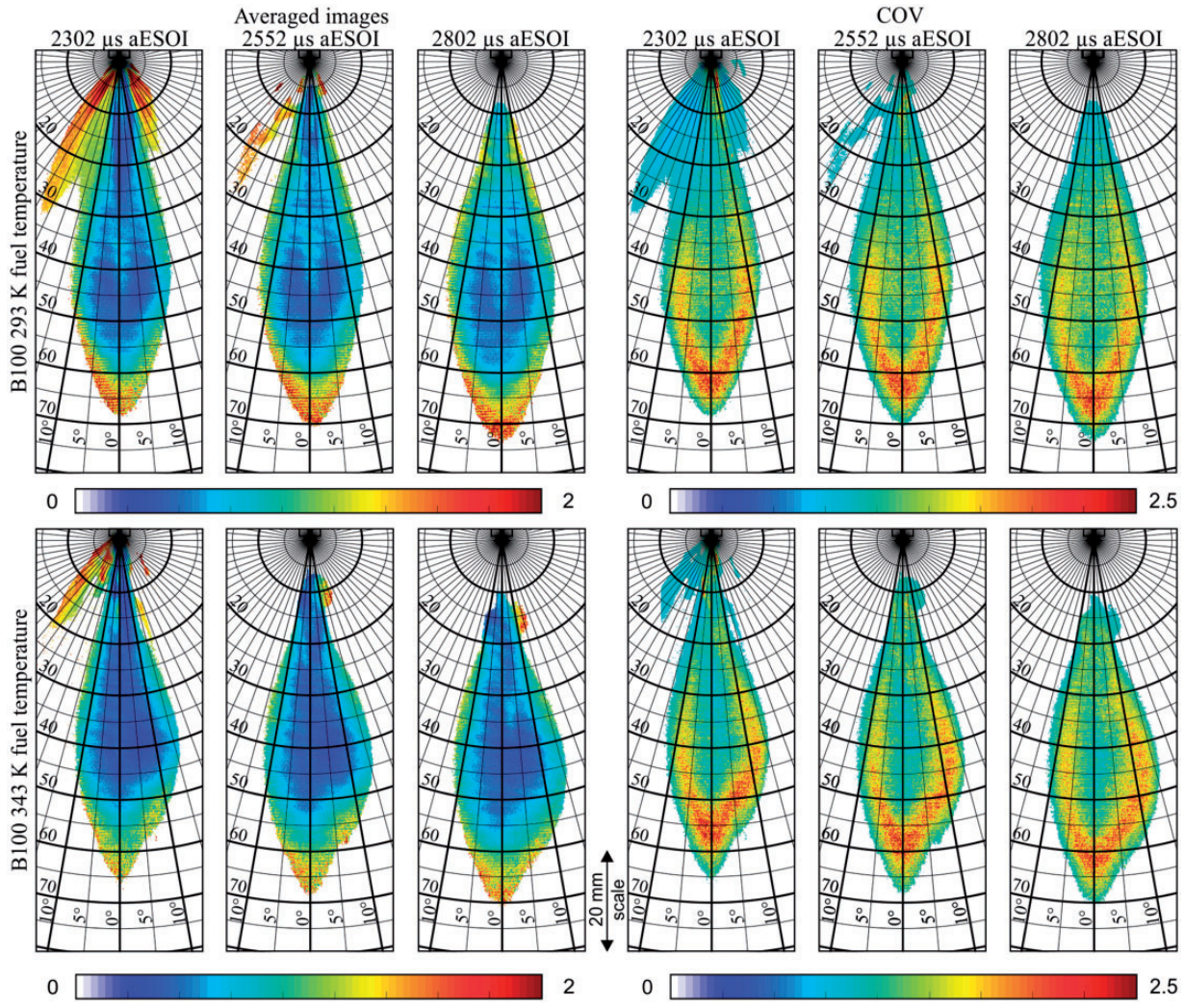

Figure 7. Comparison of averaged SLIPI-LIF/Mie ratio (left) and its corresponding COV(right) for butanol at fuel temperatures 293 and 343 K and at 2302, 2552, and 2882 µs aESOI. COV: coefficient of variation; aESOI: after electrical start of injection.

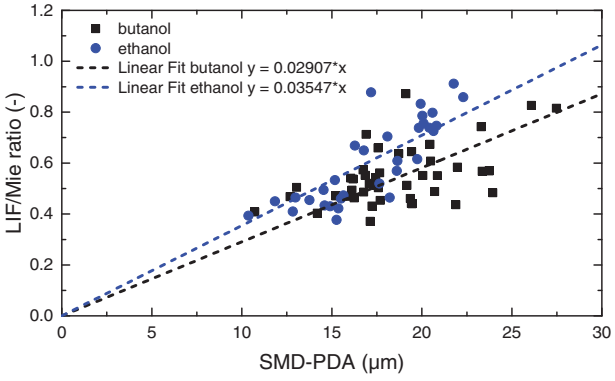

Figure 8. Calibration curve: SMD measured by PDA is plotted against SLIPI-LIF/Mie ratio of ethanol and butanol derived from data at different recording times aESOI, 298 K fuel temperature. LIF: laser-induced fluorescence; PDA: phase-Doppler anemometry; SMD: Sauter mean diameter.

smaller average droplet sizes were detected. The SMD increases toward the radial spray boundary and toward the spray front for both fuels. In the center of the spray, the SMD is in the range of 18–25 µm and at the outer radial boundary in the range of 30–40 µm for ethanol. Butanol shows larger droplet sizes especially at the spray boundary, which is explained by the less intense atomization and evaporation. The larger droplets of butanol are also confirmed by PDA measurements performed near the nozzle (at 15 mm). The histograms of the PDA measurements at this detection plane are shown in Figure 10. The whole histogram is shifted to larger droplet sizes. This is attributed due to the differences in their physical properties and not because of PDA uncertainties. For ethanol, the average SMD is 15.4 µm and for butanol it is 16.4 µm (i.e. the SMD is 6.5% larger). For butanol, droplets smaller than 5 µm were measured but more number of droplets in the

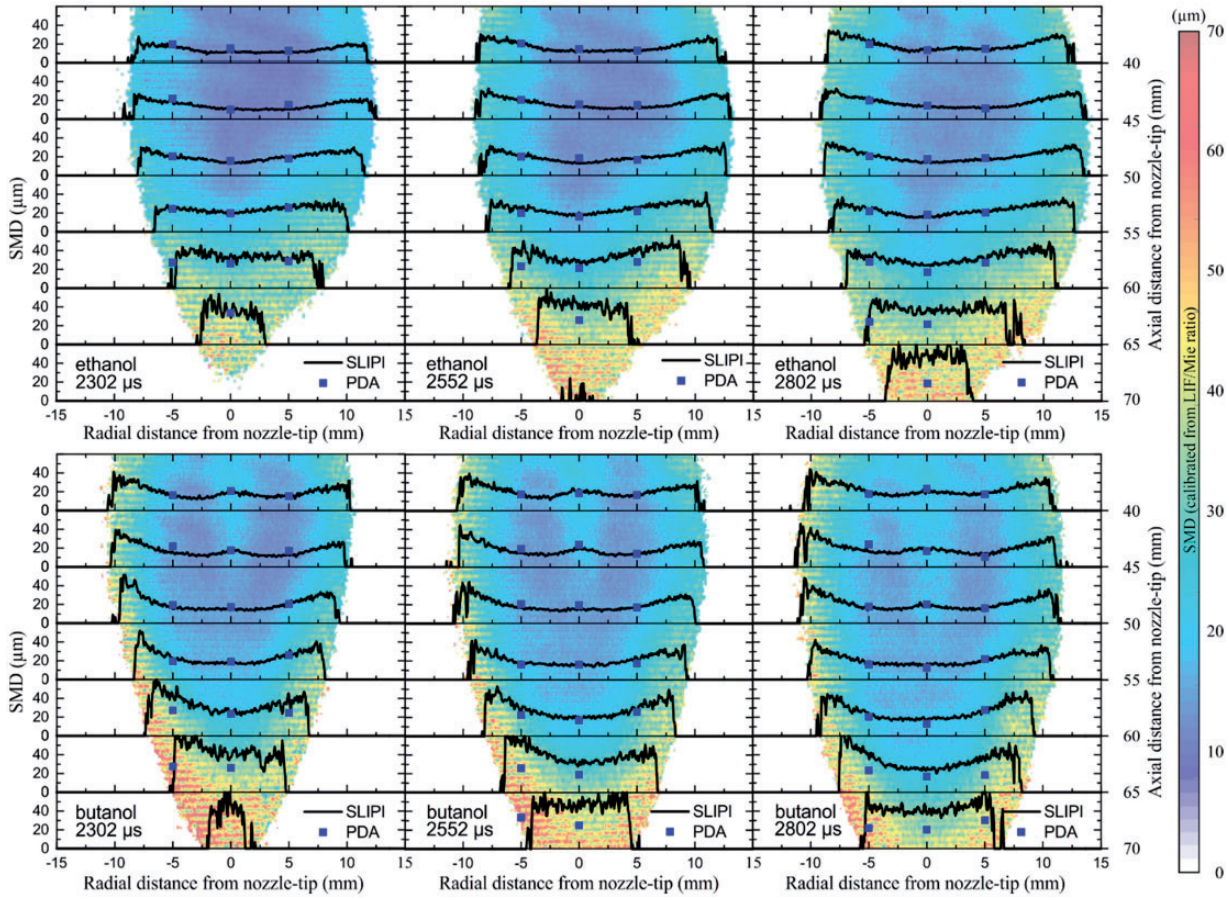

Figure 9. Droplet SMD deduced from calibrated SLIPI-LIF/Mie ratio and PDA data of ethanol (top) and butanol (bottom) at different recording times aESOI, fuel temperature 298 K. PDA: phase-Doppler anemometry; SLIPI: structured laser illumination planar imaging; SMD: Sauter mean diameter.

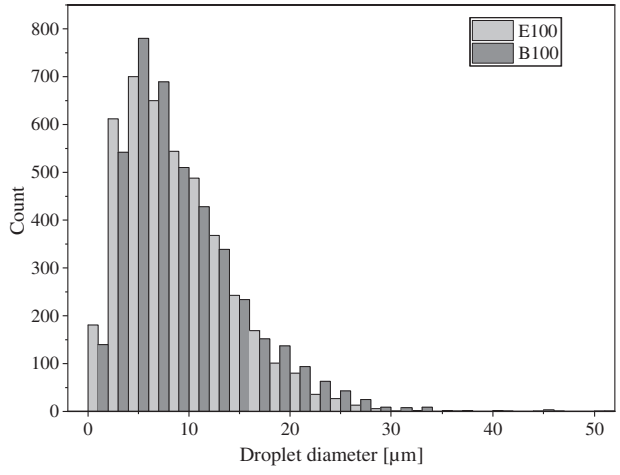

Figure 10. Droplet size distributions histogram for ethanol and butanol at 15 mm from the nozzle tip measured by PDA, fuel temperature 298 K.

range 20–30 µm exist compared to ethanol. Thus, it can be concluded that the atomization (which is dominant in these distances) should lead to the measured differences in SMD at further downstream positions and evaporation plays only a minor role.

The larger droplet size of butanol leads to larger axial droplet momentum and thus to a larger spray tip penetration in comparison to ethanol, which is very distinct at 2302 µs. The radial spray structure is even better visible in Figure 11 in which two distinct planes (40 and 55 mm below the nozzle) were extracted.

These quantitative spatially resolved data provide detailed insights into the fuel-dependent spray structure. It confirms the overall larger SMD of butanol, especially at 40 mm. Larger droplet sizes appear at the radial spray boundary for both fuels while butanol shows significantly larger droplets in these regions. This increase in SMD for butanol can be attributed

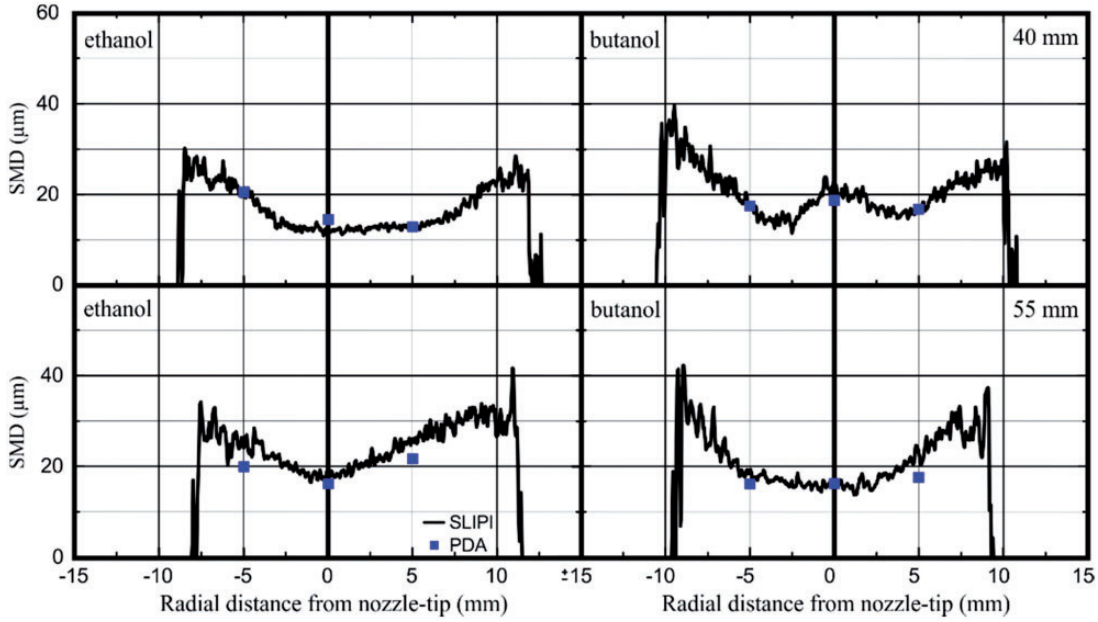

Figure 11. SMD deduced from calibrated SLIPI LIF/Mie ratio (curves) and PDA data (blue points) of ethanol (left side) and butanol (right side) at 2552 µs at 40 and 55 mm axial distance to the nozzle. PDA: phase-Doppler anemometry; SLIPI: structured laser illumination planar imaging; SMD: Sauter mean diameter.

to the delayed atomization mainly due to its lower Weber number and Reynolds number (or higher surface tension and viscosity) while at the same time the evaporation rate is lower for butanol due to its higher boiling point.

4.4. Discussion and uncertainty analysis

In this section, an uncertainty analysis is provided for the measurements presented in this work. Especially, the uncertainty shall be discussed in terms of effects of fuel evaporation that may affect the droplet temperature and the dye concentration. Furthermore, the calibration of the LIF/Mie signal using PDA will be addressed.

The SLIPI LIF/Mie technique using eosin as the dye tracer is slightly temperature dependent as shown in Figure 2. The 7% difference in LIF signal intensity (and thus a similar variation in LIF/Mie ratio) would occur for relatively large temperature changes of about 28 K. Such large temperature differences should not occur during the spray evolution as the evaporation rate is expected to be low (especially for the presented points in time between 2.3 and 2.8 ms aESOI). When assuming a maximum average temperature drop of 10 K due to evaporation cooling, the LIF signal (and similar, the LIF/Mie ratio) would vary by about 2.5%. Furthermore, in a computational fluid dynamics (CFD) simulation, the maximum cooling was about 11 K for few droplets while their average temperature decrease was about 4 K for ethanol (see Appendix 1). This means that the effect on the uncertainty of the SLIPI-LIF/Mie measurements is relatively small and it was neglected in the framework of this study. For the further investigation, the two-color LIF ratio approach will be applied for droplet thermometry in DISI spray as similar to the water spray in Mishra et al.[17] Another concern is the change in refractive index of the solution with change in its temperature, because this will also affect the PDA measurement accuracy. In order to minimize those uncertainties, the PDA detector is fixed to the Brewster angle[41] which makes the measurements insensitive to refractive index variations.

The variation in dye concentration due to spray evaporation is a fundamental issue for almost all the fuel tracer-based techniques. This effect has not been fully investigated within the framework of this study. However, Eosin-Y is a solid matter, which would not evaporate and potentially remain in the droplet. For the presented spray evolution within 500 µs (between 2.3 and 2.8 ms), it is assumed that the evaporation rate is low and not significant (which is especially true for butanol and ethanol at low fuel temperatures). In a CFD simulation of the spray (see Appendix 1), it was found that 8% of ethanol evaporates within 2.4 ms, i.e. the dye concentration would increase accordingly from 0.5 to 0.54% in average, which does not affect the measurement uncertainty significantly. However, the dye concentration of small droplets could increase due to faster evaporation and this needs further

investigation. For evaluation of this effect, measurements using a droplet generator are planned in which monodisperse droplets of different sizes will be studied at various positions downstream.

The average deviation between the SMD measured by using the SLIPI-LIF/Mie technique and PDA is about 12% in ethanol and 14% in butanol in regions 40–55 mm distance from the injector for data shown in Figure 9. The largest uncertainty is introduced by the calibration against PDA data. It could be improved by additional PDA measurement points in the spray region containing large SMD (which is complex due to the highly turbulent, unstable spray behavior and intense averaging in both the PDA and SLIPI LIF/Mie method) or another calibration method based on a droplet generator (see discussion below). In Jermy and Greenhalgh[42] the maximum uncertainty by laser sheet drop (LSD) sizing based on "conventional" LIF/Mie technique in a water cooling spray at 100–300 mm from the nozzle is specified to be ±7% (using error propagation). This is mainly determined by the calibration constant (6.5% uncertainty) and could be improved by better PDA measurements or a different method of calibration, i.e. droplet generator. However, this uncertainty does not contain effects of multiple scattering, i.e. the maximal error of LSD would further increase. It should also be mentioned that the uncertainty of the PDA measurements is about 4% in regions without significant multiple scattering.[42]

In Zeng et al.[11] the LIEF/Mie method leads to maximum deviation of 14% to the PDA-measured SMD (measurement was in the range 40–50 mm downstream the DISI nozzle), which is also mainly attributed to the uncertainty of the calibration method, the light absorption of the dye, etc. Again, the largest unknown contribution is likely the effect of the multiple scattering, which is not considered. Additionally, the effect of the temperature on the uncertainty was specified to be 7% for the studied DISI spray.[11]

As mentioned above, an improved calibration method will be conducted in future investigations using a droplet generator in which further uncertainties can be reduced. This allows calibration of single-shot spray images using single droplet data of known size so that errors introduced by averaging effects can be reduced. Furthermore, droplet temperature and dye concentration effects on the uncertainty of the LIF/Mie technique can be separated with such a device.

Finally, the effective resolution of the SLIPI LIF/Mie method can be estimated by analyzing Figures 9 and 11. There, the curves of the SMD distribution measured by SLIPI-LIF/Mie show high fluctuations in the center of the ethanol spray at 40 mm, while the average SMD is almost constant at 12.5 μm in the radial direction in a region of about 7 mm. These fluctuations are not physical and are a measure of the spatial precision. It is in the range of about ±0.56 μm of standard deviation, or 4.5% when normalized to the average SMD of 12.5 μm. The calculations are performed between −2.5 and 2.5 mm at 40 mm. For butanol, these variations are larger, namely ±0.85 μm standard deviation or 5.4% when normalized to the average SMD of 15.8 μm. In this case, the calculations are performed at 55 mm between −2.5 and 2.5 mm. This precision includes the uncertainty mainly introduced by *residual lines* in the SLIPI images, laser power fluctuations, as well as the shot noise of the cameras. Obviously, small changes in SMD can be resolved by using the SLIPI-LIF/Mie technique, see e.g. the radial SMD distribution of butanol at 40 mm at a radial distance of 0 and 5 mm. There, the SMD varies by 2 μm which is also visible in the PDA data.

5. Conclusions

In this study, DISI spray structures of the biofuels ethanol and butanol were analyzed in terms of axial and radial liquid fuel propagation and SMD using 2 p-SLIPI-LIF/Mie ratio. The SLIPI-LIF/Mie ratio was calibrated using the droplet SMD data from PDA measurements. The main results of this investigation are as follows: An increase in fuel temperature of pure ethanol results in a stronger atomization and higher evaporation rate resulting in smaller relative SMD in the spray, which also leads to reduced penetration depth and slightly increased spray width. Butanol shows larger penetration depths in comparison to ethanol, which is mainly explained by its reduced atomization because of its high surface tension and viscosity as well as lower evaporation rate. This trend is also visible in the larger SMD obtained for butanol in the whole spray region.

Butanol also shows a larger COV of the LIF/Mie ratio indicating larger cyclic variations in the spray shape, which may be explained by the changed flow behavior in the nozzle due to the high fuel viscosity, but also larger spray-induced turbulence.

Different SMD calibration curves were measured for ethanol and butanol, which is explained by the fuel-dependent LIF signal of the fuel tracer Eosin-Y used.

In general, the SMD distribution measured by PDA and the SLIPI-LIF/Mie technique shows good agreement, although average deviations of 12–14% occur for ethanol and butanol, respectively. A major uncertainty is introduced by the calibration method using PDA. Droplet evaporation weakly affects the uncertainty of the SLIPI-LIF/Mie technique at the studied conditions. The temperature dependence of the LIF signal and its effect on the uncertainty is estimated to be in the range of 2.5% because of the low evaporation rate and small

temperature drop that was also estimated in a CFD simulation of the spray.

The quantitative SMD distribution provides detailed insights into the fuel-dependent spray structure. Larger droplet sizes appear at the radial spray boundary for both fuels, while butanol shows significantly larger droplets especially in these regions. Finally, it can be concluded that the SLIPI-LIF/Mie ratio technique is suitable for investigation of the shape and structure of DISI sprays. A similar approach could be applied for diesel sprays, but the higher optical density will increase extinction effects, which makes the structural analysis within the spray more challenging. The SLIPI-LIF/Mie technique appears also suitable for other technical sprays used in power generation and process engineering, medical and agricultural applications.

A calibration of instantaneous spray images is obviously the next step, as averaging effects introduce large measurement uncertainties. This requires single droplet data, which are not available from averaged PDA data. For this purpose, subsequent calibration measurements will be done by using a droplet generator that produces a wide range of droplet sizes being relevant for DISI sprays.

Acknowledgements

We thank our colleague Dr Elias Kristensson (Lund University) for supporting the post-processing of the data and M. Sc. Giuseppe Melia (University of Calabria, Rende, Italy) for supporting the CFD simulations.

Declaration of Conflicting Interests

The author(s) declared no potential conflicts of interest with respect to the research, authorship, and/or publication of this article.

Funding

The author(s) disclosed receipt of the following financial support for the research, authorship, and/or publication of this article: The authors gratefully acknowledge the financial support by the German Federal Ministry of Food and Agriculture (BMEL) through the Agency for Renewable Resources (FNR), FKZ: 22026711. Furthermore, the authors acknowledge support by the Erlangen Graduate School in Advanced Optical Technologies (SAOT), which is funded by the German Research Foundation (DFG) in the framework of the German excellence initiative of the German Federal and State Governments to promote science and research at German universities. Dr Berrocal and Dr Mishra are funded by the European Research Council (ERC) under the European Union's Horizon 2020 research and innovation programme (Agreement No. 638546—ERC starting grant "Spray-Imaging").

References

1. Koegl M, Hofbeck B, Will S, et al. Investigation of soot formation and oxidation of ethanol and butanol fuel blends in a DISI engine at different exhaust gas recirculation rates. *Appl Energy* 2017; 209: 426–434.
2. Storch M, Pfaffenberger A, Koegl M, et al. Combustion and sooting behavior of spark-ignited ethanol–isooctane sprays under stratified charge conditions. *Energy Fuels* 2016; 30: 6080–6090.
3. Trost J, Zigan L and Leipertz A. Quantitative vapor temperature imaging in DISI-sprays at elevated pressures and temperatures using two-line excitation laser-induced fluorescence. *Proc Combust Inst* 2013; 34: 3645–3652.
4. Chen L and Stone R. Measurement of enthalpies of vaporization of isooctane and ethanol blends and their effects on PM emissions from a GDI engine. *Energy Fuels* 2011; 25: 1254–1259.
5. Storch M, Hinrichsen F, Wensing M, et al. The effect of ethanol blending on mixture formation, combustion and soot emission studied in an optical DISI engine. *Appl Energy* 2015; 156: 783–792.
6. Knorsch T, Heldmann M, Zigan L, et al. On the role of physiochemical properties on evaporation behavior of DISI biofuel sprays. *Exp Fluids* 2013; 54: 1522.
7. Zigan L, Shi J-M, Krotow I, et al. Fuel property and fuel temperature effects on internal nozzle flow, atomization and cyclic spray fluctuations of a direct injection spark ignition–injector. *Int J Engine Res* 2013; 14: 543–556.
8. Tropea C. Optical particle characterization in flows. *Annu Rev Fluid Mech* 2011; 43: 399–426.
9. Domann R and Hardalupas Y. Quantitative measurement of planar droplet Sauter mean diameter in sprays using planar droplet sizing. *Part Part Syst Charact* 2003; 20: 209–218.
10. Malarski A, Schürer B, Schmitz I, et al. Laser sheet dropsizing based on two-dimensional Raman and Mie scattering. *Appl Opt* 2009; 48: 1853–1860.
11. Zeng W, Xu M, Zhang Y, et al. Laser sheet dropsizing of evaporating sprays using simultaneous LIEF/MIE techniques. *Proc Combust Inst* 2013; 34: 1677–1860.
12. Mishra YN, Kristensson E and Berrocal E. Reliable LIF/Mie droplet sizing in sprays using structured laser illumination planar imaging. *Opt Express* 2014; 22: 4480–4492.
13. Storch M, Mishra YN, Koegl M, et al. Two-phase SLIPI for instantaneous LIF and Mie imaging of transient fuel sprays. *Opt Lett* 2016; 41: 5422–5425.
14. Zhang Z, Wang T, Jia M, et al. Combustion and particle number emissions of a direct injection spark ignition engine operating on ethanol/gasoline and n-butanol/gasoline blends with exhaust gas recirculation. *Fuel* 2014; 130: 177–188.
15. Bladh H, Hildingsson L, Gross V, et al. Quantitative soot measurements in an HSDI diesel engine. In: *Thirteenth int symp on applications of laser techniques to fluid mechanics*, Lisboa, Portugal, 26-29 June 2006.
16. Neil MAA, Juškaitis R and Wilson T. Method of obtaining optical sectioning by using structured light in a conventional microscope. *Opt Lett* 1997; 22: 1905–1907.
17. Mishra YN, Abou Nada F, Polster S, et al. Thermometry in aqueous solutions and sprays using two-color LIF and structured illumination. *Opt Express* 2016; 24: 4949–4963.

18. Kristensson E, Berrocal E and Aldén M. Extinction coefficient imaging of turbid media using dual structured laser illumination planar imaging. *Opt Lett* 2011; 36: 1656–1658.
19. Kristensson E, Berrocal E, Wellander R, et al. Structured illumination for 3-D Mie imaging and 2-D attenuation measurements in optically dense sprays. *Proc Combust Inst* 2011; 33: 855–861.
20. Kristensson E, Berrocal E and Aldén M. Two-pulse structured illumination imaging. *Opt Lett* 2014; 39: 2584–2587.
21. Mishra YN, Kristensson E, Koegl M, et al. Comparison between two-phase and one-phase SLIPI for instantaneous imaging of transient sprays. *Exp Fluids* 2017; 58: 110.
22. Le Gal P, Farrugia N and Greenhalgh DA. Laser sheet dropsizing of dense sprays. *Opt Laser Technol* 1999; 31: 75–83.
23. Domann R and Hardalupas Y. Spatial distribution of fluorescence intensity within large droplets and its dependence on dye concentration. *Appl Opt* 2001; 40: 3586–3597.
24. Frackowiak B and Tropea C. Numerical analysis of diameter influence on droplet fluorescence. *Appl Opt* 2010; 49: 2363–2370.
25. Frackowiak B and Tropea C. Fluorescence modeling of droplets intersecting a focused laser beam. *Opt Lett* 2010; 35: 1386–1388.
26. Charalampous G and Hardalupas Y. Numerical evaluation of droplet sizing based on the ratio of fluorescent and scattered light intensities (LIF/Mie technique). *Appl Opt* 2011; 50: 1197–1209.
27. Charalampous G and Hardalupas Y. Method to reduce errors of droplet sizing based on the ratio of fluorescent and scattered light intensities (laser-induced fluorescence/Mie technique). *Appl Opt* 2011; 50: 3622–3637.
28. Berrocal E, Kristensson E, Hottenbach P, et al. Quantitative imaging of a non-combusting diesel spray using structured laser illumination planar imaging. *Appl Phys B* 2012; 109: 683–694.
29. Barone TL, Storey JME, Youngquist AD, et al. An analysis of direct-injection spark-ignition (DISI) soot morphology. *Atmos Environ* 2012; 49: 268–274.
30. Dean JA. *Lange's handbook of chemistry*. 15th edition, New York: McGraw-Hill Companies, 1999.
31. Yetter RA and Glassman I. *Combustion*. Amsterdam: Academic Press, 2008.
32. Technology, NIoSa. NIST Chemistry WebBook, 2017.
33. Rheims J, Köser J and Wriedt T. Refractive-index measurements in the near-IR using an Abbe refractometer. *Meas Sci Technol* 1997; 8: 601.
34. El-Kashef H. The necessary requirements imposed on polar dielectric laser dye solvents. *Phys B Condens Matt* 2000; 279: 295–301.
35. Hiroyasu H and Arai M. *Structures of fuel sprays in diesel engines*. SAE International, SAE number 900475, 1990.
36. Baumgarten C. *Mixture formation in internal combustion engine*. Berlin, Heidelberg: Springer, 2006.
37. Heldmann M. *Untersuchungen zur Massen-, Geschwindigkeits- und Impulsverteilung in Freistrahl- und Doppelstrahl-Sprays für die Benzindirekteinspritzung (english translation; Investigation of mass, velocity and momentum distribution of free jet and twin jet sprays for DISI applications)*. Dissertation. FAU University Erlangen-Nuremburg, 2015.
38. Aleiferis PG, Serras-Pereira J, van Romunde Z, et al. Mechanisms of spray formation and combustion from a multi-hole injector with E85 and gasoline. *Combust Flame* 2010; 157: 735–756.
39. Chakraborty M and Panda AK. Spectral behaviour of Eosin Y in different solvents and aqueous surfactant media. *Spectrochim Acta Part A Mol Biomol Spectrosc* 2011; 81: 458–465.
40. Storch M, Lind S, Will S, et al. Influence of ethanol admixture on the determination of equivalence ratios in DISI engines by laser-induced fluorescence. *Appl Opt* 2016; 55: 8532–8540.
41. Schünemann E, Fedrow S and Leipertz A. Droplet size and velocity measurements for the characterization of a DI-diesel spray impinging on a flat wall. SAE paper 982545, 1998.
42. Jermy MC and Greenhalgh DA. Planar dropsizing by elastic and fluorescence scattering in sprays too dense for phase Doppler measurement. *Appl Phys B* 2000; 71: 703–710.
43. Nordin N. *Complex chemistry modeling of diesel spray combustion*. PhD thesis, Sweden: Chalmers University of Technology, 2001.
44. Zigan L, Ammon M, Schmitz I, et al. Investigation of fuel effects on spray atomization and evaporation studied for a multi-hole DISI injector with a late injection timing. *SAE Int J Fuels Lubr* 2012; 5: 254–264.

Appendix 1

A simplified CFD simulation was conducted for estimation of the evaporation rate and the resulting droplet temperature using the 3D-CFD-Code OpenFOAM 2.4. One jet of the five-hole injector is modeled as no significant liquid jet-to-jet interactions were observed in the experiments. A Euler–Lagrange spray model with a transient Reynolds-averaged Navier–Stokes approach was set up including all relevant submodels for the spray processes for a realistic spray representation.[43] The enhanced Taylor-analogy-breakup model was applied for atomization, the ''trajectory'' model was used for considering droplet collision, the ''stochastic dispersion'' model for turbulent droplet dispersion, and the ''infinite diffusion model'' for evaporation. Furthermore, droplet drag (''sphere drag'' model) was considered and for simulation of turbulence, the ''RNG k–epsilon'' model was applied. About 10,000 parcels were injected for representation of the spray behavior. The spray model was calibrated regarding spray shape (especially penetration) as well as droplet size distribution using the SLIPI-LIF/Mie ratio and PDA data, aforementioned. Further details of the

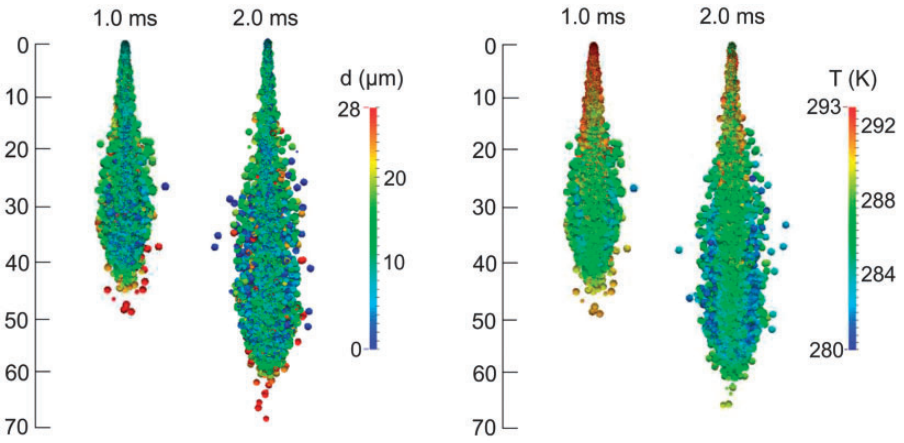

Figure 12. Simulated droplet size and droplet temperature of the ethanol spray for a single jet at two points in time 1 and 2 ms aSOI. The droplets are shown for a central plane in the jet.

general model calibration procedure can be found elsewhere.[44] In the CFD simulation, it was found that 8% (by mass) of ethanol evaporates within 2.4 ms after start of injection (aSOI), which leads to a reduction of the droplet size and temperature. In Figure 12, the spray shape is displayed for ethanol at two points in time in terms of droplet size (left) and droplet temperature (right).

At earlier time points aSOI (1 ms), the maximum temperature reduction of the droplets is about 9 K. Later on, the maximum droplet cooling was about 11 K for few droplets while the average temperature reduction was about 4 K. The maximum temperature reduction occurs in the outer radial spray boundary region in which the interaction with ambient air is highest and thus, the evaporation rate is maximal as well. For comparison, also the simulated droplet size is visualized showing very similar droplet sizes at the center of the spray while few larger droplets occur at the axial and radial spray boundary in accordance to the SMD distribution measured by the SLIPI LIF/Mie technique.